RSC Advances

RSC Publishing

PAPER

View Article Online
View Journal | View Issue

Flexible poly(vinyl alcohol-*co*-ethylene)/modified MMT moisture barrier composite for encapsulating organic devices

Cite this: *RSC Advances*, 2013, **3**, 12831

Sindhu Seethamraju,[a] Praveen C. Ramamurthy*[ab] and Giridhar Madras[a]

Received 1st April 2013,
Accepted 9th May 2013

DOI: 10.1039/c3ra41557k

www.rsc.org/advances

Flexible, nano-composite moisture barrier films of poly(vinyl alcohol-*co*-ethylene) with surface modified montmorillonite fabricated by solution casting were used to encapsulate organic devices. The composite films were characterized by FTIR, UV-visible spectroscopy and SEM imaging. Thermal and mechanical properties of the composite films were studied by DSC and UTM. Calcium degradation test was used to determine the transmission rate of water vapour through the composite films, which showed a gradual reduction from $\sim$0.1 g m^{-2} day^{-1} to 0.0001 g m^{-2} day^{-1} with increasing modified montmorillonite loading in the neat copolymer. The increase in moisture barrier performance is attributed to the decreased water vapour diffusivity due to matrix–filler interactions in the composite. The accelerated aging test was carried out for non-encapsulated and encapsulated devices to evaluate the efficiency of the encapsulants. The encapsulated devices exhibited longer lifetimes indicating the efficacy of the encapsulant.

Introduction

Recent developments in organic electronics[1–4] indicate a broad scope for research to develop highly flexible, moisture- and oxygen-impermeable barrier materials.[5,6] Barrier materials have been extensively used in food and pharmaceutical packaging industries. However, the sensitivity of organic devices like organic light emitting diodes (OLEDs) and organic photovoltaics (OPVs) towards moisture and oxygen[6–9] demands much higher barrier requirements. For such applications, oxygen transmission rates (OTR) $<10^{-5}$ cm^3 m^{-2} day^{-1} and water vapour transmission rates (WVTR) $<10^{-6}$ g m^{-2} day^{-1} are required.

Techniques like atomic layer deposition and chemical vapour deposition of inorganic oxides over organic layers[10–13] are commonly used for achieving high barrier encapsulants. However, they are not cost effective and not suitable for large area and large scale manufacturing. Layered polymer composite films may be economically viable because of the opportunity for roll processing. Therefore, polymer nanocomposites/hybrid materials are extensively being investigated as ultra-low barrier materials.[14–16] Multilayered/stacked layers of polymers are used commercially[17,18] but they do not meet the ultra-high barrier requirement of devices. In order to improve the barrier properties of such multilayered polymer films, each individual polymer layer can be designed separately by incorporating nano-getter materials/exfoliating inorganic nano-platelets. Therefore, in this study, the suitability of using composite films of poly(vinyl alcohol-*co*-ethylene) and surface modified montmorillonite as an effective barrier layer is evaluated.

Poly(vinyl alcohol-*co*-ethylene) (EVOH) is one of the highly impermeable polymers to oxygen with OTR $\sim$ 0.01 cm^3 m^{-2} day^{-1} [19] because of the presence of polar –OH and excellent self-association.[20] It has been commercially used in various multilayered packaging films as an oxygen barrier.[21–23] The ethylene content in the copolymer defines the extent of crystallinity and thus the permeability.[24,25] However, in the presence of moisture, the interactions between H_2O molecules and –OH groups of EVOH result in plasticization of the polymer chains of EVOH leading to an increase of permeability.[26,27]

Various nanofillers are commercially available for enhancing thermal, mechanical, UV and barrier properties of the matrix polymer of which clays occupy a major fraction. The addition of nanoclay to the neat polymer will result in the enhancement of the barrier properties by providing a tortuous pathway to the permeant.[28] Subsequently to the Toyota patent,[29] various polymer clay composites have been examined for their optimal properties.[30,31] Clays are hydrophilic in nature and most polymers (being hydrophobic) are immiscible with each other. Surface modified clays with alkylammonium and alkylphosphonium ions render miscibility with hydrophobic polymers due to increased wettability.[30] Organic modification further increases the gallery spacing depending on the alkyl chain length.[32]

[a]*Center for Nanoscience and Engineering, Indian Institute of Science, Bangalore, India. E-mail: praveen@materials.iisc.ernet.in; Fax: +91-80-2360-0472; Tel: +91-80-2293-2627*

[b]*Department of Materials Engineering, Indian Institute of Science, Bangalore, India*

EVOH–clay composites have been previously investigated for thermal, mechanical and oxygen barrier properties[33–35] and used for food packaging applications. In this work, commercially available highly exfoliated modified clay has been used as the nanofiller with an EVOH polymer matrix at various compositions. The modified filler was chosen in such a way that oxygen barrier properties of EVOH would not be affected at high humidity conditions as the modified clay layers hold the polymer chains together and even absorb water. Hence, a single composite layer would act as a sacrificial barrier capable of decreasing the WVTR which even helps to decrease the oxygen permeability. The permeation behaviour of water molecules through the composites was evaluated from calcium degradation test and the effectiveness as a barrier was determined by encapsulating organic devices under accelerated aging conditions.

Experimental methods

Materials

Commercial poly(vinyl alcohol-*co*-ethylene) containing 38% ethylene and montmorillonite (MMT) clay surface modified with octadecylamine (15–35 wt%) and aminopropyltriethoxysilane (0.5–5 wt%) were obtained from Sigma Aldrich Ltd (St. Louis, MO). Dimethylsulfoxide (DMSO), tetrahydrofuran (THF) and tetrachloroethylene (CCl_4) solvents of 99.9% purity were purchased from local suppliers (S.D. Fine Chemicals, India Ltd.) and used without further purification.

Sample preparation

EVOH-modified MMT composite films were prepared by the solution casting technique. 3.0 g of EVOH was dissolved in 18 ml of DMSO at 80 °C by continuously stirring on a magnetic stirrer. After dissolution, modified MMT was added in 1, 2 and 5 wt% to the EVOH solution and dispersed for 24 h by continuous stirring and then sonicated for 30 min. These dispersed solutions were poured onto a Teflon coated mould and cast at 110 °C. Similarly, a neat copolymer film (as a control film) was cast without adding modified MMT. All the films were dried under vacuum at 20 mmHg for 48 h to remove the residual solvent and stored in a desiccator. The films were of 235 ± 15 μm thickness. Thus-prepared films were designated as EVOH 0 for neat copolymer film (*i.e.*, no modified MMT) and EVOH 1, EVOH 2 and EVOH 3 for the composite films with 1, 2 and 5 wt% of modified MMT added, respectively.

Characterization methods

Modified MMT powder sample and all the sample films were characterized using a Thermo-Nicolet 6700 IR spectrometer in the range 400 to 4000 cm^{-1} with 4 cm^{-1} resolution. The BET surface area of the modified MMT was determined using a SmartSorb 92/93 surface area analyzer. Before the analysis, the samples were dried at 120 °C for 2 h to remove the adsorbed moisture from the surface. UV-visible characterization of all the sample films was carried out on a Perkin Elmer (model Lambda-35) spectrometer in the wavelength range of 230–1100 nm. Thermal properties of the neat polymer and composite films were determined using a Mettler Toledo (DSC 822^e) instrument at a heating rate of 10 °C min^{-1} in nitrogen atmosphere. Two consecutive heating and cooling cycles were run from 30 to 220 °C and 220 to 30 °C respectively. The second heating cycle was used for analysis. Tensile analysis for all the films was carried out by considering 3 samples from each film on a Mecmeisin Micro Universal Testing Machine, using 10 kN load cell at a rate of 25 mm min^{-1} following the ASTM D882-12 standard. The scanning electron microscopy (SEM) images for cryogenically fractured films were obtained from an ESEM QUANTA 200. The fractured surfaces sputter coated with gold were used for SEM imaging. The X-ray analysis for all the sample films and modified MMT was performed using a D8 Advance Bruker AXS X-ray diffractometer at a scan rate of 1° min^{-1}.

A density gradient column was constructed following the ASTM D1505 standard to determine the density of the composite films. The 1 m column was filled with THF (886 kg m^{-3}) and CCl_4 (1590 kg m^{-3}), with decreasing density compositions from the bottom to the top of the column. The mixtures of THF/CCl_4 (v/v) 100/0, 80/20, 70/30, 60/40, 50/50, 40/60, 30/70, 25/75, 20/80, 10/90, 5/95, 0/100 were slowly poured into the column from the sides of column wall avoiding turbulence. Standard density calibrated glass beads (H & D Fitzgerald Ltd., St. Asaph, UK) and the samples were dropped into the column one after another. The column was calibrated for density using the standard bead positions.

Water vapour permeability determination

Calcium degradation test was used for the determination of WVTR as well as to calculate the moisture diffusivities through the neat and composite films. This was determined by following the change in resistance of the calcium with time[36,37] under humid conditions. 200 nm thick calcium (of density = ∂) was thermally evaporated at the center 1 cm × 1 cm ($l \times b$) onto a 2 cm × 2 cm ($l \times w$) clean glass slide. On either side of the calcium, aluminium electrodes of 300 nm thick were deposited, as shown in Fig. 1.

The glass slide was sealed with the sample film using room temperature curable epoxy (Lapox L12 Atul Industries, India Ltd.). Thus, the sealed device acts as a moisture sensor. When moisture permeates through the film, thermally deposited calcium starts oxidizing. As calcium degrades, the change in resistance (R) with time (t) is measured using a digital

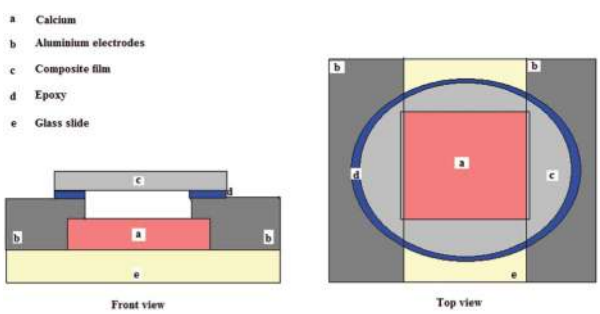

Fig. 1 Schematic of calcium degradation test setup.

multimeter. Water vapour permeated through the barrier film was calculated using eqn (1):

$$\mathrm{WVTR} = -2\frac{M_{\mathrm{H2O}}}{M_{\mathrm{Ca}}}\partial\rho\left(l/b\right)\frac{\mathrm{d}\left(1/R\right)}{\mathrm{d}t} \quad (1)$$

where M_{H_2O} and M_{Ca} correspond to the molar weights of water and calcium respectively. Eqn (1) is valid only if the resistivity of calcium (ρ) is constant with varying thickness. It can be observed that the resistivity of calcium is dependent on the film thickness.[38] It is found to be constant only above the thickness of 100 nm for calcium. Therefore, WVTR through the composite films was calculated considering the change in thickness from 200 nm to 100 nm. An experiment to verify the negligible WVTR through the cured glue was conducted by sealing a similarly calcium deposited glass slide with glass using the glue. All the above steps were carried under inert atmosphere, inside the Mbraun glove box (ultra-high purity nitrogen atmosphere, $H_2O < 10$ ppm, $O_2 < 10$ ppm) integrated with a thermal evaporator. Sealed glass slides were placed in a controlled humid environment of RH = 95% ($\pm$3%) and at 35 °C ($\pm$0.2 °C) inside a Kaleidoscope programmable humidity chamber.

Accelerated aging studies of encapsulated diodes

Organic devices were fabricated using 1.5 wt% of poly(3-hexylthiophene) (P3HT) in dichlorobenzene. 100 μl of P3HT solution was spin coated onto an ITO coated glass slide. These coated glass slides were annealed at 110 °C for 10 min and aluminium electrodes were thermally deposited using a shadow mask. The structure of the device was ITO/P3HT/Al. Thus-fabricated devices were sealed at the edges with sample films using epoxy as shown in Fig. 2.

Using a Keithley source meter (Model 2420), the *I–V* characteristics for all the devices were measured initially and after exposure to a humid environment of 95% RH at 35 °C for investigating the device performance under accelerated conditions.

Results and discussion

MMT clays are arranged in stacked layers of tetrahedral silicate and octahedral aluminate sheets. When the gallery spacing between the sheets is increased, due to organic modification, this results in the formation of intercalated and exfoliated clays. This provides a more tortuous pathway to the penetrant through the polymer composite by increasing the diffusion length. Moreover, functionalization helps to increase their compatibility with the organic polymer phase. The increase of interactions results in better compatibility. This decreases the free volume in the polymer/clay composite resulting in the decrease of the free volume available for penetrant permeation through the composite.

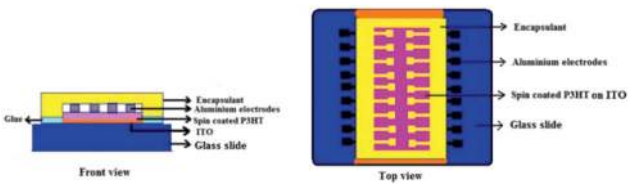

Fig. 2 Schematic of encapsulated organic device.

Characterization

The BET surface area of modified MMT was found to be 22 m^2 g^{-1} whereas unmodified montmorillonites generally have surface areas of ~750 m^2 g^{-1}.[30] Functionalization of the montmorillonite surface with alkylated amines decrease the BET surface area as the surface is occupied by the alkyl groups.[39] This will induce hydrophobicity[30] in the hydrophilic clay which helps the dispersion of the filler in the matrix.

When modified MMT is dispersed in EVOH copolymer, the alkyl chains of the amine functional group and the ethylene part of the copolymer are compatible because of the van der Waals interactions. This helps in exfoliating clay layers, further increasing the gallery spacing. The amine groups of the modified clay and the hydroxyl groups of the copolymer interact forming hydrogen bonds. This forms a strongly interacting matrix–filler composite decreasing the free volume which can be evidenced from the density profile as given in Table 1. As the density of modified MMT was 233 kg m^{-3}, the density of the composites predicted by the rule of mixtures (given in Table 1) is much lower than the determined experimental density. This can be attributed to the increased packing of the polymer chains because of the EVOH-modified MMT interactions in the composites.

For the neat polymer film, a density of 1186 kg m^{-3} was observed while that value increased to 1219 kg m^{-3} for EVOH 3. This increase can be attributed to the increased modified MMT integration with the EVOH matrix.

Thermal and FTIR characterization

DSC analysis (Fig. 3) of the neat and composite films for glass transition (T_g) and melting (T_m) temperatures are tabulated in Table 1. The glass transition temperatures increased by 4 °C from EVOH 0 to EVOH 3. With increasing modified MMT content in the matrix, the thermal energy required for the segmental motion of the polymer chains increased, due to the increased packing. The melting temperature of all the composites increased by 4 °C with respect to that of the neat polymer. The increase of the melting temperature is due to the increase in chain stiffening or rigidity of the polymer chains. With the addition of modified MMT to the neat polymer, due to the increased affinity between the matrix and filler, the rigidity of the composites increases resulting in higher T_m values. The percentage crystallinity of the neat and composite films is determined considering the 100% crystalline enthalpy of 157.8 J g^{-1}.[40] From Table 2, it can be observed that the crystallinity of the composite films increased from 35.8% for the neat copolymer to 46.9% for the composite film EVOH 3. With increasing modified MMT content in the EVOH matrix, the crystallinity of the matrix increased due to the increased alignment of the polymer chains. The increase in T_g and crystallinity further suggests the decrease in free volume

Table 1 Melting properties and densities of all the composite films

Sample	Glass transition (°C)	Onset of melting (°C)	Peak melting point (°C)	Density (kg m^{-3})	
				Calculated	Experimental
EVOH 0	53.8 ± 0.1	162	169.3 ± 0.1	1186	1186 ± 1
EVOH 1	54.3 ± 0.1	166	173.8 ± 0.2	1176	1191 ± 2
EVOH 2	55.4 ± 0.2	168	174.2 ± 0.1	1167	1207 ± 2
EVOH 3	57.8 ± 0.2	169	174.4 ± 0.2	1138	1219 ± 3

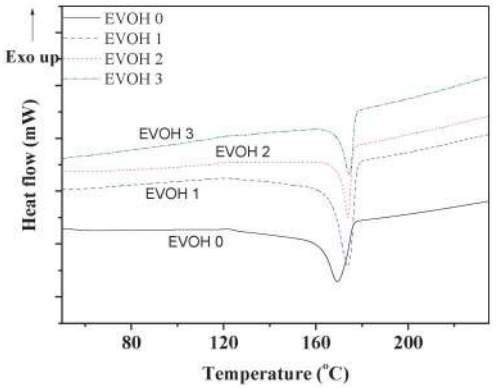

Fig. 3 DSC analysis of all the composites.

availability with the addition of modified MMT to EVOH, which increases the barrier properties of EVOH.

From the FTIR spectra for modified MMT as shown in Fig. 4, the peaks observed at 3634 cm^{-1}, 2924 and 2852 cm^{-1}, and 1023 cm^{-1} correspond to stretching of O–H, modifying hydrocarbons[41] of amine and silane functionalization and Si–O–C of organic silane respectively. The peaks at 625 cm^{-1}, 525 cm^{-1} and 470 cm^{-1} indicate the presence of oxides of aluminium, magnesium and silicon, respectively. The peak at 3435 cm^{-1} is due to the presence of intra-molecular hydrogen bonded O–H groups. When the modified MMT is dispersed in EVOH, these –OH functional groups overcome intra-molecular attractions and interact with EVOH polymer chains by intermolecular hydrogen bonding, forming a compatibilized exfoliated structure.[42] From the FTIR spectra for the composites (Fig. 4), the peak corresponding to hydrogen bonded O–H stretching around 3346 cm^{-1} in the neat polymer (EVOH 0) film is hardly visible, but the broadened band ranging from 3580 cm^{-1} to 3200 cm^{-1} can be attributed to the stretching of varying strengths of a large number of hydrogen bonded O–H groups. The broadened region was also an overlap of various C–H stretching peaks in the copolymer from 3200 cm^{-1} to 2890 cm^{-1}. The intensity of absorption increased over the broadened region from 3580 cm^{-1} to 3200 cm^{-1} suggesting strengthening as well as increase in the extent of hydrogen bonding interactions in all the composite films with respect to that observed in EVOH 0 because of the addition of modified MMT to the neat polymer. A similar increase in hydrogen bonding absorption band was also observed for a blend of poly(vinyl alcohol) and poly(ethylene oxide).[43] The increase in hydrogen bonding increases the cohesive energy density thereby decreasing the free volume available, as observed from the increase in melting temperature and density.

SEM imaging

From the SEM images in Fig. 5 (a, b) for the fractured surface of the composite film, it can be observed that addition of modified MMT to the neat polymer increased the extent of crack formation as compared to the neat polymer. When the film is cryogenically fractured, the chains are frozen in their native state and broken apart. The pattern of cracks observed on the fractured surface suggests the intensity of interactions between the polymer chains.

Therefore the increase in cracks and sub-cracks can be attributed to the increased packing of the polymer chains due to interfacial interactions because of hydrogen bonding interactions between the hydroxyl groups of the polymer matrix and the amine group of modified MMT layers as well as the increased compatibility of the ethylene content in the copolymer and the octadecyl chains of the modified MMT.

Mechanical characterization

The stress/strain plots for all the composite films are shown in Fig. 6. The tensile strength at break (Table 3) decreases with increasing modified MMT content. The percentage elongation was >100% for all the films and it decreased with increase in modified MMT loading. However, the tensile yield strength and elongation at yield were independent of the modified MMT content. This would be satisfactory for the composite films to be used as flexible barrier materials for organic device encapsulation.

Table 2 Percentage crystallinity of the neat and composite films

Sample	Melting point (°C)	ΔH (J g^{-1})	Percentage crystallinity (%) = (100 × $\Delta H/\Delta H_{100\ cry}$)
EVOH 0	169.3	56.59	35.8
EVOH 1	173.8	57.99	36.7
EVOH 2	174.2	61.79	39.1
EVOH 3	174.4	74.02	46.9

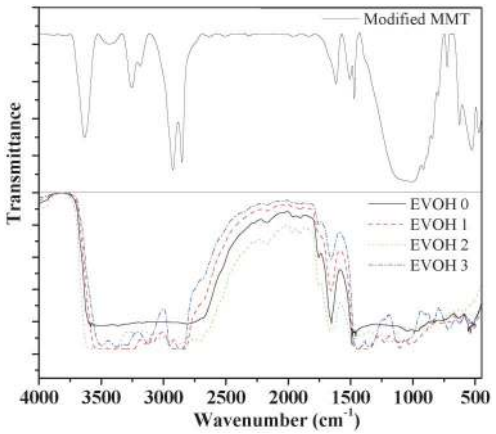

Fig. 4 FTIR spectra of modified MMT and all the composites.

UV-visible and X-ray characterization

The UV-visible spectroscopic analysis shown in Fig. 7 suggests that all the films exhibit ~60% transparency in the visible region (400–700 nm) and this decreases in the UV region (230–400 nm).

From the X-ray analysis as shown in Fig. 8, a peak was observed only for the modified MMT powder at $2\theta = 4.3^\circ$. This indicates that the modified MMT which was used in the composite had a gallery spacing of 22 Å. No peaks were observed from 1° to 10° for any of the composite films. This could be due to the exfoliated/intercalated nano-clay layers in the polymer or due to the random arrangement of the modified MMT in the matrix.

WVTR and moisture diffusivity determination for the composites

From the calcium degradation test, the variations of the normalized conductance (R_o/R) of calcium with time for all the sample films at 95 ± 3% RH and $T = 35 \pm 0.2$ °C were plotted in Fig. 9. The WVTR through the films was calculated for all the composite films and this is shown in Fig. 10.

The average WVTR values over different time intervals for all compositions are given in Table 3. It can be observed that the average permeability value gradually decreased from EVOH 0 to EVOH 3 by more than two orders of magnitude. The two order decrease in magnitude of WVTR can be attributed to all the previously discussed various factors, such as choosing appropriate filler and matrix, possibility of interactions between the polymer and filler and geometry of the filler arrangement in the composite. If modified MMT layers were randomly arranged and not exfoliated, then there could not have been this increase in the barrier properties, which is due to the increased tortuosity.

All the tests were conducted on uniformly deposited calcium at the same time under similar conditions. It can also be observed from Fig. 9 that with increasing modified MMT content, the time required for complete degradation of calcium increased indicating the increased barrier properties with respect to the neat polymer. Moreover, as the clays are capable of absorbing water by clustering H_2O molecules, the WVTR values were observed to be decreasing after 5000 s. The initial time required for the water molecules to start clustering is higher for the EVOH 3 composite (4000 s) as compared to EVOH 2 (2000 s) due to the presence of more MMT layers in EVOH 3 than in EVOH 2. Hence, the initial values of WVTR are higher for EVOH 3, which decreased by one order subsequently.

The diffusion coefficients for water vapour (D) through the composite and the neat polymer films were calculated by considering the film as a two-dimensional sheet of thickness s. The concentration of water vapour on one side (facing calcium) of the film is assumed to be zero initially, whereas on the other side, it is considered to be maintained at concentration c corresponding to 95% RH and 35 °C.

$$\frac{Q}{sc} = \frac{Dt}{s^2} - \frac{1}{6} - \frac{2}{\Pi^2}\sum_{n=1}^{\infty}\frac{(-1)^n}{n^2}\exp\left(-\frac{Dn^2\Pi^2 t}{s^2}\right) \qquad (2)$$

Eqn (2) was solved for water vapour diffusion coefficient using the cumulative amount of water vapour passing through the composite film obtained from calcium degradation test.[44]

It can be observed from Table 4 that the diffusivity of water vapour decreased with increasing clay content. Moreover, the diffusivities for EVOH/modified MMT composite films were less by one order than those obtained previously for poly(vinyl alcohol)/ZnO composite films,[45] which show good barrier properties. As a rule of thumb, values of WVTR obtained at accelerated conditions of 95% RH and 35 °C are expected to be two orders lower than that obtained at ambient conditions.

Accelerated weathering studies

Current–voltage (I–V) characteristics for all the Schottky structured devices were measured initially and after accelerated ageing (95% RH at 35 °C). After ageing for time t, the percentage reduction in current density with respect to the initial current density for all the devices was calculated from I–V characteristics in the 0 to 1 V range. The percentage change in current density was calculated for each device at a particular voltage (V) using eqn (3). The change in current density after a particular time "t" of accelerated aging, over the complete 0–1 V range (as shown in Fig. 11) was averaged to determine the average device performance and to compare with other devices.

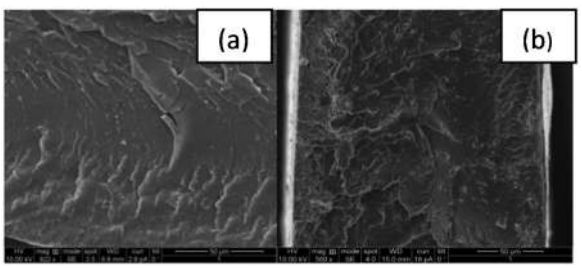

Fig. 5 SEM image of fractured film surface of (a) EVOH 0 and (b) EVOH 3.

Table 3 Tensile properties of all the composite films

	EVOH 0	EVOH 1	EVOH 2	EVOH 3
Tensile strength at break (MPa)	31.5 ± 0.5	28.8 ± 0.2	28.7 ± 0.3	24.1 ± 0.7
Elongation at break (%)	167 ± 5	167 ± 10	130 ± 5	100 ± 5
Tensile yield strength (MPa)	24.3 ± 0.5	26.5 ± 0.9	26.3 ± 0.7	24.7 ± 0.3
Elongation at yield (%)	10.8 ± 0.3	9.5 ± 0.5	9.7 ± 0.5	9.5 ± 0.5

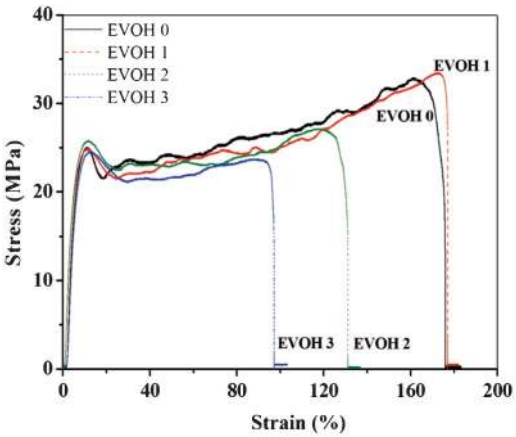

Fig. 6 Tensile analysis of the composite films.

$$\%\ \text{Change in current density} = \frac{\text{initial current density (at } V) - \text{current density at time } t \text{ (at } V)}{\text{initial current density (at } V)} \times 100 \quad (3)$$

It can be observed from Fig. 11 (a) that after 20 min, there was a 98 ± 1% change in current density for the non-encapsulated device and ~60% for the device encapsulated with the neat polymer film (EVOH 0). This shows that the bare polymer film itself was able to reduce the device characteristics degradation to some extent. However, no significant reduction of current density was observed for devices encapsulated with EVOH 1 to 3. From Fig. 11 (b) it can be observed that, after 4 h of accelerated ageing, the change in current density was about 30% and was 95% for the diodes encapsulated with EVOH 3 and EVOH 0, respectively. This implies that the device lifetime increased with increasing modified MMT content in the matrix polymer. Increasing the modified MMT content increased the diffusion path for the water vapour molecule to pass through the film, which is also suggested by lower water vapour diffusivity values for the composites.

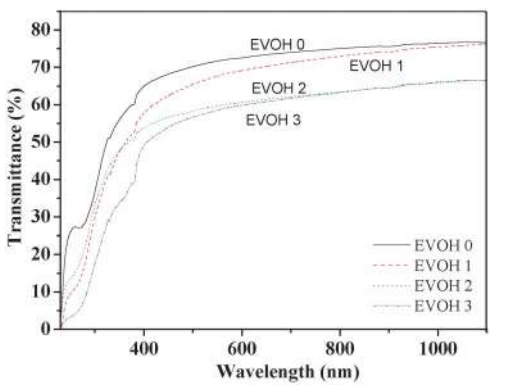

Fig. 7 UV-visible analysis of the composite films.

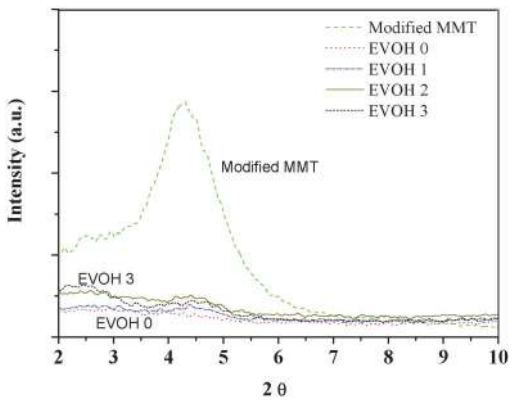

Fig. 8 X-ray analysis of modified MMT and all the composites.

Conclusions

Poly(vinyl alcohol-*co*-ethylene)/modified MMT composite films were fabricated. Due to the interactions between EVOH and dispersed modified MMT layers in the composite matrix, the

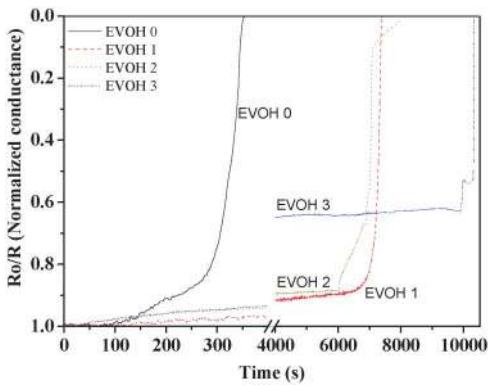

Fig. 9 Calcium degradation with time from change in resistance for the composite films.

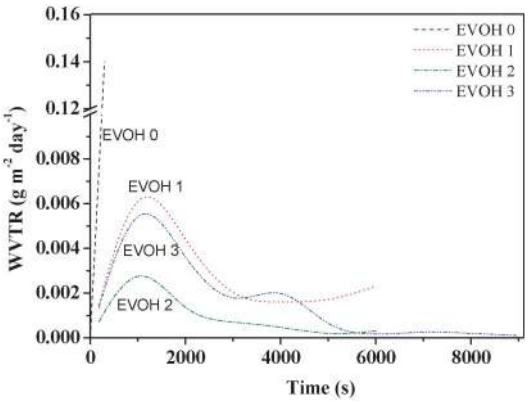

Fig. 10 Water vapour permeabilities for composite films determined from calcium degradation test.

density of the composites increased, and the thermal properties improved. These flexible composites were found to be stable with improved moisture barrier properties as compared to the neat polymer film. This implies that the composite matrix did not get plasticized even at 95% RH due to strong matrix–filler interactions. It was further observed that the device lifetime increased by 10 times for the EVOH 3 encapsulated device, compared with that of the non-encapsulated device under accelerated conditions. These results validate the effectiveness of the composite as a water vapour barrier for organic device encapsulation. Moreover, this composite layer can be used in layered architecture, *i.e.* embedding this composite film between two highly impermeable moisture barrier polymers would further help in achieving much higher moisture barrier properties as well as prolonged device lifetimes.

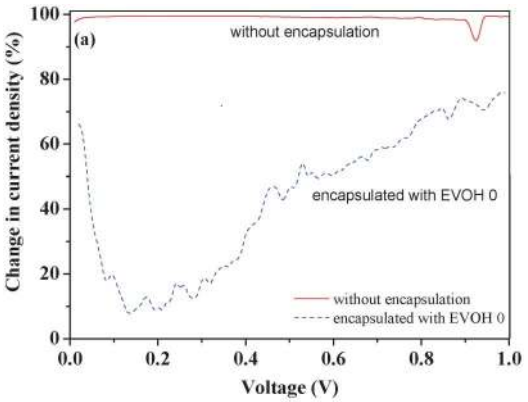

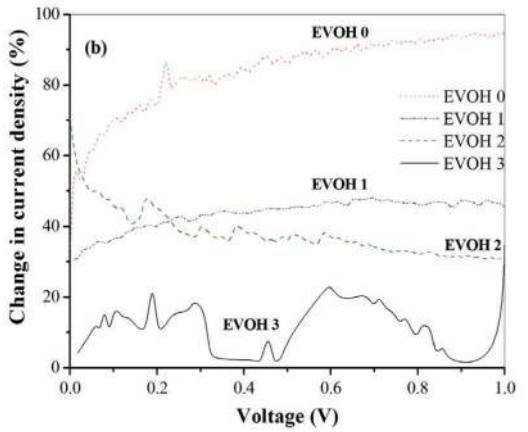

Fig. 11 Percentage change in device performance for (a) non-encapsulated and EVOH 0 encapsulated device after 20 min, and (b) comparing device performances for encapsulated devices after 4 h of accelerated ageing.

Table 4 Permeability properties of all the composite films determined from Ca test

	WVTR (g m^{-2} day^{-1})			
Time (s)	EVOH 0	EVOH 1	EVOH 2	EVOH 3
0–1000	0.14	0.0081	0.0039	0.0073
1000–2000		0.0042	0.0009	0.0033
2000–3000		0.0016	0.0007	0.0012
3000–4000		0.0016	0.0005	0.0026
4000–5000		0.0016	0.0001	0.0003
5000–6000		0.0023	0.0003	0.0001
6000–7000				0.0003
7000–8000				0.0002
8000–9000				0.0001
Diffusion coefficient $\times$ 10^{12} (m^2 s^{-1})	35	2.6	2.2	1.6

Acknowledgements

The authors gratefully acknowledge the financial support from DST No SR/S3/ME/022/2010-(G) and by the Ministry of Communication and Information Technology under a grant for the Centre of Excellence in Nanoelectronics, Phase II. The authors thank Mr. Satyajit Gupta for helpful discussions.

Notes and references

1 M. C. Choi, Y. Kim and C. S. Ha, *Prog. Polym. Sci.*, 2008, **33**, 581.
2 H. Spanggaard and F. C. Krebs, *Sol. Energy Mater. Sol. Cells*, 2004, **83**, 125.
3 S. K. Swathi, K. Ranjith, P. Kumar and P. C. Ramamurthy, *Sol. Energy Mater. Sol. Cells*, 2012, **96**, 101.
4 P. C. Ramamurthy, W. R. Harrell, R. V. Gregory, B. Sadanadan and A. M. Rao, *Synth. Met.*, 2003, **137**, 1497.
5 N. Grossiord, J. M. Kroon, R. Andriessen and P. W. M. Blom, *Org. Electron.*, 2012, **13**, 432.
6 K. Norrman, S. A. Gevorgyan and F. C. Krebs, *ACS Appl. Mater. Interfaces*, 2009, **1**, 102.
7 K. Kawano, R. Pacios, D. Poplavskyy, J. Nelson, D. D. C. Bradley and J. R. Durrant, *Sol. Energy Mater. Sol. Cells*, 2006, **90**, 3520.

8 H. B. Yang, Q. L. Song, C. Gong and C. M. Li, *Sol. Energy Mater. Sol. Cells*, 2010, **94**, 846.
9 A. Seemann, T. Sauermann, C. Lungenschmied, O. Armbruster, S. Bauer, H. J. Egelhaaf and J. Hauch, *Sol. Energy*, 2011, **85**, 1238.
10 P. E. Burrows, G. L. Graff, P. M. Martin, M. K. Shi, M. Hall, E. Mast, C. Bonham, W. Bennett and M. B. Sullivan, *Displays*, 2001, **22**, 65.
11 G. Dennler, C. Lungenschmied, H. Neugebauer, N. S. Sariciftci, M. Latreche, G. Czeremuszkin and M. R. Wertheimer, *Thin Solid Films*, 2006, **512**, 343.
12 D. S. Wuu, T. N. Chen, C. C. Wu, C. C. Chiang, Y. P. Chen, R. H. Horng and F. S. Juang, *Chem. Vap. Deposition*, 2006, **12**, 220.
13 Y. C. Han, C. Jang, K. J. Kim, K. C. Choi, K. H. Jung and B. S. Bae, *Org. Electron.*, 2011, **12**, 609.
14 S. Gupta, P. C. Ramamurthy and M. Giridhar, *Polym. Chem.*, 2011, **2**, 221.
15 Z. Wu, L. Wang, C. Chang and Y. Qiu, *J. Phys. D: Appl. Phys.*, 2005, **38**, 981.
16 J. Gaume, C. T. Gueho, S. Cros, A. Rivaton, S. Therias and J. L. Gardette, *Sol. Energy Mater. Sol. Cells*, 2012, **99**, 240.
17 Multilayer with Surlyn. http://www.itwinsulation.com/pabco-childers/Data_Sheets/polysurlyn_moisture_barrier.pdf.
18 Multilayered commercial films biaxially extruded. http://catalog.ides.com/docselect.aspx?I=38903&E=208202&DOC=DOWTDS&DS=123&DK=STD&DC=en.
19 EVAL Americas. Technical Bulletin No. 110. Gas barrier properties of EVALTM Resins. http://www.eval-americas.com/media/36916/tb_no_110.pdf.
20 M. M. Coleman, X. Yang, H. Zhang and P. C. Painter, *J. Macromol. Sci., Part B: Phys.*, 1993, **32**, 295.
21 O. G. Schroeder, *US Patent*, 4,254,169, 1981.
22 S. G. Henry, *US Patent*, 4928474, 1990.
23 T. Harinder and M. Planeta, *US Patent*, 6218024, 2001.
24 D. Cava, C. Sammon and J. M. Lagaron, *Appl. Spectrosc.*, 2006, **60**, 1392.
25 T. Iwanami and Y. Hirai, *Tappi J.*, 1983, **66**, 85.
26 Z. Zhang, I. J. Britt and M. A. Tung, *J. Polym. Sci., Part B: Polym. Phys.*, 1999, **37**, 691.
27 Z. Zhang, I. J. Britt and M. A. Tung, *J. Appl. Polym. Sci.*, 2001, **82**, 1866.
28 K. Yano, A. Usuki, A. Okada, T. Kurauchi and O. Kamigaito, *J. Polym. Sci., Part A: Polym. Chem.*, 1993, **3**, 2493.
29 A. Okada, Y. Fukushima, M. Kawasumi, S. Inagaki, A. Usuki, S. Sugiyama, T. Kurauchi and O. Kamigaito, *US Patent*, 739007, 1988.
30 S. Pavlidou and C. D. Papaspyrides, *Prog. Polym. Sci.*, 2008, **33**, 1119.
31 J. U. Calderon, B. Lennox and M. R. Kamal, *Appl. Clay Sci.*, 2008, **40**, 90.
32 V. V. Ginzburg, C. Singh and A. C. Balazs, *Macromolecules*, 2000, **33**, 1089.
33 L. Cabedo, E. Gimenez, J. M. Lagaron, R. Gavara and J. J. Saura, *Polymer*, 2004, **45**, 5233.
34 H. M. Jeong, B. C. Kim and E. H. Kim, *J. Mater. Sci.*, 2005, **40**, 3783.
35 S. S. Lee, M. H. Hur, H. Yang, S. Lim and J. Kim, *J. Appl. Polym. Sci.*, 2006, **101**, 2749.
36 R. Paetzold and A. Winnacker, *Rev. Sci. Instrum.*, 2003, **74**, 5147.
37 J. H. Choi, Y. M. Kim, Y. W. Park, J. W. Huh and B. K. Ju, *Rev. Sci. Instrum.*, 2007, **78**, 064701.
38 P. Renucci, L. Gaudart, J. P. Petrakian and D. Roux, *Phys. Rev. B*, 1982, **26**, 5416.
39 H. He, Q. Zhou, W. N. Martens, T. J. Kloprogge, P. Yuan, Y. Xi, J. Zhu and R. L. Frost, *Clays Clay Miner.*, 2006, **54**, 689.
40 M. L. Cerrada, E. Perez, J. M. Perena and R. Benavente, *Macromolecules*, 1998, **31**, 2559.
41 R. A. Vaia, R. K. Teukolsky and E. P. Giannelis, *Chem. Mater.*, 1994, **6**, 1017.
42 I. J. Chin, T. T. Albrecht, H. C. Kim, T. P. Russell and J. Wang, *Polymer*, 2001, **42**, 5947.
43 C. Sawatari and T. Kondo, *Macromolecules*, 1999, **32**, 1949.
44 J. Crank, *The Mathematics of Diffusion*, second edn., Oxford University Press, Oxford, UK, 1975.
45 S. Gupta, S. Sindhu, K. A. Varman, P. C. Ramamurthy and G. Madras, *RSC Adv.*, 2012, **2**, 11536.

